

27 to retreat ~ 18.5 km by the end of this century leading to a total mass loss of ~ 2068 Gt (5.7 mm sea
28 level rise equivalent). Despite the relative success of the model in simulating the recent behavior of
29 the glacier, the model does not simulate winter calving events that have become relatively more
30 important.

31 1 Introduction

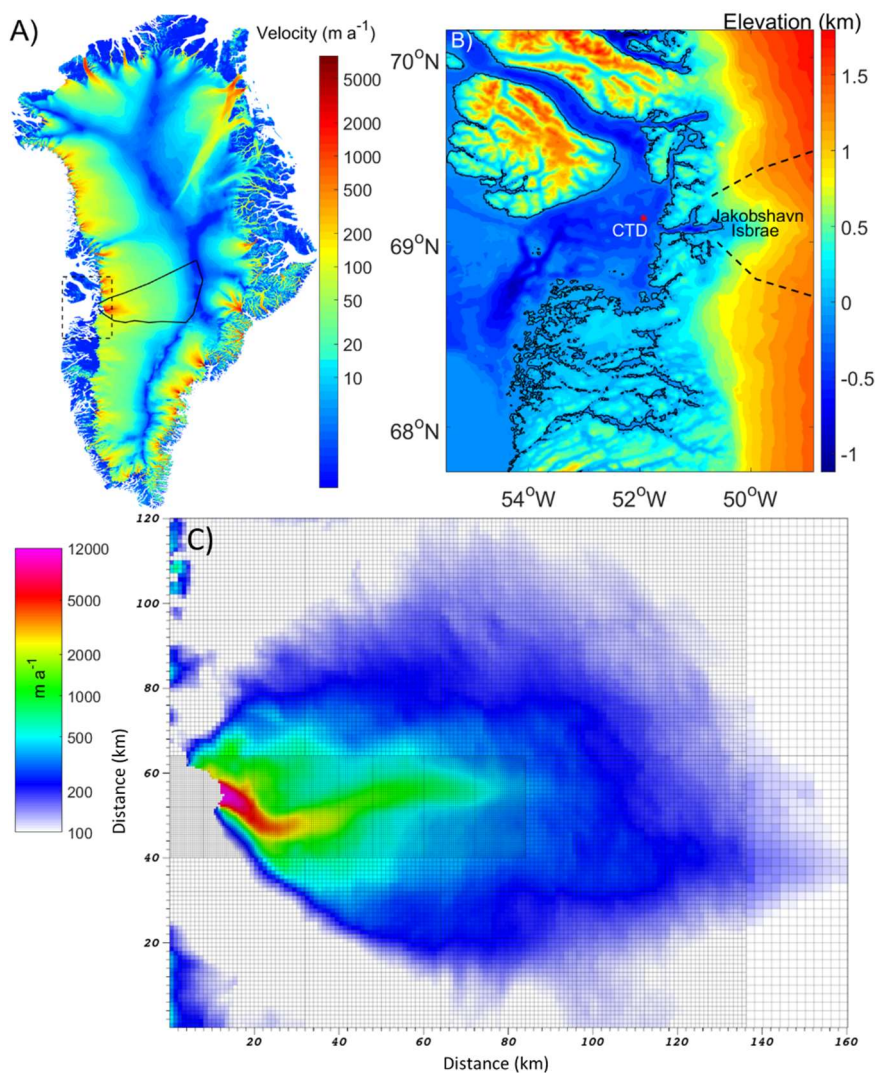


Figure 1. A) Greenland ice sheet flow speeds from Joughin et al. (2018), with the Jakobshavn drainage basin outlined by the solid black line and the area shown in panel B by the dashed box. B) Ilulissat Fjord and Disko Bay bathymetry from Jakobsson et al. (2012), with the CTD (Conductivity Temperature Depth) site used for ocean temperature

here marked by the red star. C) Example of the mesh used with finest resolution of 500 m with modeled velocities at the beginning of 2004.

32 Jakobshavn Isbræ (Fig. 1) is Greenland's largest and fastest outlet glacier, with transient speeds of
33 up to 17 km a^{-1} (Joughin et al., 2014). Jakobshavn Isbræ drains $\sim 6.5 \%$ of the Greenland Ice sheet
34 (Krabill et al., 2000), and it alone contributed $\sim 1 \text{ mm}$ to global sea-level rise between 2000 and
35 2011 (Howat et al., 2011). Since 1997, measurements indicate that the water entering Ilulissat Fjord
36 where Jakobshavn Isbræ terminates, is about $1.1 \text{ }^\circ\text{C}$ warmer than it was during 1987-1991 (Holland
37 et al., 2008). This rise in water temperature coincided with the onset of dramatic thinning, speedup
38 and retreat of Jakobshavn Isbræ. By 2003 its velocity near the grounding line had reached ~ 12.6
39 km a^{-1} , more than double that of 1992, and the ice shelf in the fjord had disintegrated (Joughin et
40 al., 2004). From 2005 to 2007, as it retreated inland, seasonal fluctuations in velocity 4 km inland
41 from the calving front amounted to $\pm 1 \text{ km a}^{-1}$. The winter slowdowns and summer accelerations
42 occurred in tandem with the calving front winter advance and summer retreat. By 2012 the seasonal
43 velocity fluctuations 4 km upstream from the calving front were nearly $\pm 8 \text{ km a}^{-1}$ and the grounding
44 line of Jakobshavn Isbræ had reached the bottom of a sub-glacial bedrock trough after years of
45 down-slope migration (Joughin et al., 2014).

46 Before 1997, Jakobshavn had a $\sim 15 \text{ km}$ long ice shelf in front of its grounding line and experienced
47 submarine melting on its ice-ocean interface (Amundson et al., 2010). After 1998 the terminus
48 became more crevassed, coinciding with acceleration of the glacier, implying that weakened
49 buttressing had triggered its dramatic speed-up. A thinning rate of $230 \pm 50 \text{ m a}^{-1}$ between the
50 summers of 1984 and 1985 was deduced from photogrammetric surveys, with 98% contributed by
51 submarine melting (Motyka et al., 2011). The ice shelf thickened during the mid-1990s followed by
52 progressive thinning after 1997 (Motyka et al., 2011). From 1997 to 2008, the average ocean
53 temperature was 1.1°C higher than during the period 1980 – 1991, which raised its thinning rate

54 substantially, affecting the whole ice shelf that eventually collapsed in 2003. Many lines of evidence
55 suggest that warm water was responsible for the submarine melting beneath the ice mélange and
56 ice-shelf, brought by a buoyancy-driven, overturning circulation in Ilulissat fjord (Gladish et al.,
57 2015).

58 Jakobshavn, in common with most outlet glaciers in Greenland, flows through a narrow, deeply
59 incised bedrock trough at a much faster rate than the ice surrounding it (Joughin et al., 2010). Gravity
60 surveys suggest a deep layer of soft till underlies much of the Jakobshavn trough (Block and Bell,
61 2011). This soft bed provides almost no resistance to ice flow and basal shear stress maps show that
62 most of the gravitational driving force on the glacier is balanced by lateral drag (Shapiro et al.,
63 2016).

64 Basal drag decreased from 1995 to 2006 (Habermann et al., 2013), possibly due to fast thinning that
65 reduced the effective pressure, that is the ice overburden minus water pressure, at the bed. The
66 effective pressure distribution under the glacier is important to basal drag and approaches zero at
67 the grounding line as the ice begins to float. Several sliding parameterizations (also termed sliding
68 relations or sliding laws) have been used in the literature that assume basal drag depends on sliding
69 speed (so-called Weertman sliding (Weertman, 1957)), or on effective pressure (Schoof, 2010;
70 Gagliardini et al., 2014). Tsai et al. (2015) introduced a combined Weertman and Coulomb sliding
71 law based on effective pressures with a boundary layer at the grounding line; this has a higher scaling
72 of ice flux with grounding-line thickness compared with the Weertman. However, in the Jakobshavn
73 case, both Weertman and Coulomb sliding produce very similar fluxes because the basal shear
74 stresses along the main trough are typically only 2% of the driving force (Shapiro et al., 2016).

75 Simulations using a flow-band model with a crevasse-depth-based calving parameterization (Vieli
76 et al., 2011) demonstrated that loss of buttressing from the weakening mélange or enhanced

77 submarine melting could have triggered the dramatic changes seen in Jakobshavn Isbræ at the end
78 of the 20th century. Later work (Muresan et al., 2016), using a simple calving model with
79 dependence on the strain field at the terminus was able to reproduce the inter-annual retreat of
80 Jakobshavn Isbræ until 2009, when the terminus arrived at the beginning of the reverse sloping bed.
81 But retreat after 2010 was not captured by their model, and neither were the seasonal fluctuations
82 in terminus position. Bondzio et al. (2018) applied a similar calving model that removes any ice
83 where tensile stress exceeds a threshold, as simulated with a SSA (Shallow Shelf Approximation)
84 model, regardless of ice thickness. To represent seasonal fluctuation of front position, their stress
85 threshold is a stepwise constant function in time with low values in summer. After calibration, their
86 model can closely reproduce the observed behavior from 1985 to 2018 when forced only with ocean
87 temperatures.

88 In this paper we use a three-dimensional ice-flow model with a treatment of calving that successfully
89 tracks the seasonal terminus position and its retreat into the over-deepened basin. We use historic
90 observations of ocean temperature as forcing and ice shelf melting rate to scale submarine melting
91 rates for our model and thence make future projections. Our aim is to track the evolution of
92 Jakobshavn Isbræ through the 21st century under a specific climate forcing scenario. In Section 2
93 we describe the approach and calibration of our model, Section 3 shows the simulations for the
94 period to 2100 under the IPCC RCP4.5 scenario (Moss et al., 2010), Section 4 is a discussion of our
95 results with reference to other studies and suggestions for improvements, and we conclude in
96 Section 5.

97 **2 Methods and data**

98 **2.1 Ice sheet model**

99 We model Jakobshavn Isbræ using the BISICLES ice sheet dynamics model that is based on the
100 vertically integrated stress balance formulation of Schoof and Hindmarsh (2010), which treats
101 longitudinal and lateral stresses as depth-independent, but allows for vertical shear in the nonlinear
102 rheology (Cornford et al., 2013). BISICLES is particularly useful for Jakobshavn Isbræ as it uses
103 block-structured finite volume discretization with adaptive mesh refinement (Cornford et al., 2013)
104 allowing for high resolution modeling of critical sections of the glacier. Jakobshavn Isbræ is fed by
105 a ~ 400 km long and extensive drainage basin (Fig. 1), but the fast flow area is only around 10 km
106 in width. Our highest mesh resolution of 500 m is used to cover the whole fast-flow-area including
107 the shear margin (Fig. 1c), while the rest of the glacier is modeled at 1000 m resolution.

108 We assume the floating part of Jakobshavn Isbræ to be in hydrostatic equilibrium, thus the upper
109 surface elevation s is

$$110 \quad s = \max \left[h + b, \left(1 - \frac{\rho_i}{\rho_w} \right) h \right], \quad (1)$$

111 where ρ_i and ρ_w are the densities of ice (917 kg m^{-3}) and ocean water (1027 kg m^{-3}), h is ice
112 thickness and b is bedrock elevation relative to sea level. The ice thickness evolves in time as

$$113 \quad \frac{\partial h}{\partial t} + \nabla \cdot [\mathbf{u}h] = M_s - M_b, \quad (2)$$

114 where M_s , M_b are surface mass balance (SMB) and submarine melt rate respectively and \mathbf{u} is the
115 depth-independent horizontal velocity. No basal melting over the grounded area is allowed. The
116 velocity \mathbf{u} satisfies an approximate stress balance equation (Schoof and Hindmarsh, 2010)

117 $\nabla \cdot [\phi h \bar{\mu} (2\dot{\epsilon} + 2\text{tr}(\dot{\epsilon})\mathbf{I})] - \boldsymbol{\tau}^b = \rho_i g h \nabla s, \quad (3)$

118 where \mathbf{I} is the identity tensor, s is the ice surface elevation, g is the acceleration due to gravity, $\dot{\epsilon}$ is
 119 the horizontal strain-rate tensor defined by

120 $\dot{\epsilon} = \frac{1}{2} [\nabla \mathbf{u} + (\nabla \mathbf{u})^T], \quad (4)$

121 and $\boldsymbol{\tau}^b$ is the basal shear stress. The vertically integrated effective viscosity $h\bar{\mu}$ is given by

122 $h\bar{\mu}(x, y) = \int_{s-h}^s \mu(x, y, z) dz, \quad (5)$

123 where the vertically varying effective viscosity μ includes a contribution from vertical shear and
 124 satisfies

125 $2\mu A(T) (4\mu^2 \dot{\epsilon}^2 + |\rho_i g (s - z) \nabla s|^2)^{(n-1)/2} = 1, \quad (6)$

126 where n is the flow rate exponent, set to 3 in the current study, and $A(T)$ is the rate factor, dependent
 127 on the ice temperature T through an Arrhenius law (Cuffey and Paterson, 2010). ϕ is a stiffening
 128 factor estimated by solving an inverse problem (Cornford et al., 2015) using measured surface
 129 velocities.

130 We use a viscous Weertman sliding relation to define the basal friction:

131 $\boldsymbol{\tau}^b = \begin{cases} -C |\mathbf{u}|^{m-1} \mathbf{u} & \text{if } \frac{\rho_i}{\rho_w} h > -b \\ 0 & \text{otherwise} \end{cases}, \quad (7)$

132 and here we assume a linear relation taking $m=1$. The basal traction coefficient $C(x, y)$ is estimated
 133 simultaneously with the stiffening factor ϕ by solving the inverse problem (Cornford et al., 2015).
 134 C and ϕ are adjusted iteratively to reduce the misfit with a set of 2010 surface velocity observations
 135 (Joughin et al. 2010). We hold the fields C and ϕ constant over time throughout our simulations,

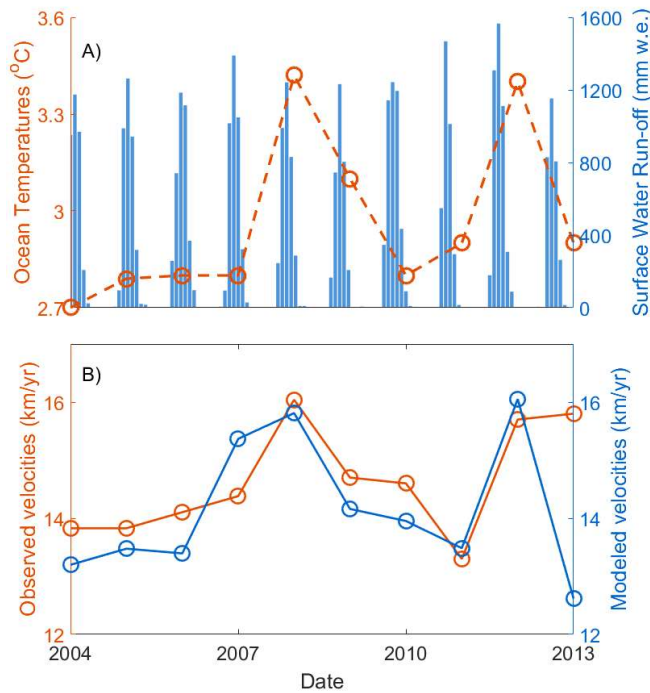
136 although they must actually change as the glacier retreats. We also do not thermomechanically
 137 couple the model, but use a constant ice temperature of -10°C .

138 Reflection boundary conditions were applied at the edge of the domain:

139
$$\mathbf{u} \cdot \mathbf{n} = 0, \quad \mathbf{t} \cdot \nabla \mathbf{u} \cdot \mathbf{n} = 0, \quad \nabla h \cdot \mathbf{n} = 0, \quad (8)$$

140 where \mathbf{n} is normal to a boundary and \mathbf{t} is parallel to it. Normal stress across the calving front is equal
 141 to the hydrostatic water pressure there:

142
$$\mathbf{n} \cdot [\phi h \bar{\mu} (2\dot{\epsilon} + 2\text{tr}(\dot{\epsilon})\mathbf{I})] - \boldsymbol{\tau}^b = \frac{1}{2} \rho_i g \left(1 - \frac{\rho_i}{\rho_w}\right) h^2 \mathbf{n}. \quad (9)$$



143

144 **Figure 2. A) Time series of observed ~300 m deep ocean temperature (red) from near the mouth of**
 145 **Ilulissat fjord (See Fig. 1 for location). Blue bars are simulated monthly surface water run-off from**
 146 **the MAR regional surface mass and energy balance model (Alexander et al. 2016). B) Measured**
 147 **ice front annual mean ice flow speeds (red) from Joughin et al. (2010), compared with our modeled**
 148 **speeds (blue).**

149 **2.2 Forcing**

150 Local ocean circulation in Ilulissat fjord driven by buoyancy plume brings deep water from outside
151 to the grounding line of Jakobshavn, and renews the fjord waters within 90 days in summer (Gladish
152 et al., 2015). Generally, Jakobshavn’s fjord is ~ 800 m deep but with a sill of only ~ 200 m depth at
153 its entrance. The deepest water outside the sill can flow over the sill and reach the grounding line of
154 Jakobshavn (Gladish et al., 2015). We use 300 m depth ocean temperatures collected from a CTD
155 site close to the mouth of Ilulissat fjord (Fig. 1) as an approximation of ocean temperatures near the
156 glacier grounding line (Gladish et al. 2015). A positive correlation ($r=0.74$, $p<0.05$) exists between
157 deep ocean temperatures and flow speed near the terminus of Jakobshavn Isbrae (Fig. 2) from 2004
158 onwards. There is no significant correlation prior to 2004, the ice shelf period. As a working
159 hypothesis we assume that the correlation since 2004 reflects the effects of the sea ice and iceberg
160 mélangé in the fjord on the flow speed near the terminus: a warmer ocean reduces mélangé and sea
161 ice thickness and therefore buttressing. There appears to be no lag between the glacier acceleration
162 and change in deep ocean temperature, suggesting mélangé response times are faster than 1 year.
163 When the ice shelf was present lags in the system were likely longer, accounting for the lack of
164 correlation between ocean temperatures and glacier flow speed prior to 2004. It is also possible that
165 ocean temperatures reflect changes in surface runoff and basal lubrication for sliding, but we
166 consider that the runoff more strongly affects calving mechanisms as discussed later. We therefore
167 modify the driving force (Eq. 3) on the grid cells next to the calving front by multiplying by a factor
168 α that is linearly related to ocean temperature (T) as a means of representing the buttressing effects
169 of the ice mélangé in the fjord.

$$170 \nabla \cdot [\phi h \bar{\mu} (2\dot{\epsilon} + 2\text{tr}(\dot{\epsilon})\mathbf{I})] + \boldsymbol{\tau}^b = \alpha \cdot \rho_i g h \nabla s, \quad (10)$$

$$171 \alpha = \alpha_1 + \alpha_2 \cdot T, \quad (11)$$

172 The coefficients α_1 and α_2 are tunable with limits based on observations as discussed later in Section
173 2.4. This approach is similar to Nick et al. (2013), which also alters the stress balance at calving
174 front. Our buttressing parameterization gives a longitudinal resistance that is 18% of the driving
175 force at calving front (Eq. 10), for the instance of 2004.

176 We use a crevasse based calving parameterization (Benn et al., 2007; Nick et al., 2013) that calves
177 ice where the crevasse penetration depth (D_s) is greater than upper surface elevation. D_s is defined
178 as

$$179 \quad D_s = \frac{S}{g \cdot \rho_i} + \frac{\rho_w}{\rho_i} \cdot R \cdot \beta, \quad (12)$$

180 where S is the magnitude of extensional stress, R is surface water run-off, and β is a tuning scalar.
181 We estimate runoff from the 25 km resolution regional climate model, MAR, (Alexander et al. 2016),
182 driven by the ERA-Interim reanalysis (Dee et al., 2011).

183 We characterize submarine melting as a linear function of ocean forcing

$$184 \quad M_b = \gamma T_f, \quad (13)$$

185 where T_f is the far field ocean forcing temperature, taken in Disko Bay (CTD in Fig. 1), relative to
186 pressure melting temperature under the ice shelf. Thus T and T_f are related simply by ice depth and
187 salinity. We derive γ (Section 2.3) from the 1985 observed submarine melt rate of 1 ± 0.2 m day⁻¹
188 beneath the ice shelf of Jakobshavn Isbræ, when Disko Bay ocean temperatures were 4.2°C warmer
189 than the pressure melting point at the bottom of the floating ice shelf (Motyka et al. 2011). We test
190 the sensitivity of the modeled glacier to uncertainty in submarine melt rate in section 2.4.

191 We force Jakobshavn Isbræ in the 21st century using SMB and run-off from the 11 km resolution
192 RACMO model (Van Angelen et al., 2013) driven by the RCP4.5 scenario (Moss et al. 2010). The

193 run-off values are averaged over the nine grid points nearest to the terminus of Jakobshavn (69.1°N,
194 50.0°W). In general we use RACMO products to drive the model, however they only span the period
195 of 2006-2009. For the period 2004-2014, SMB and surface water run-off forcing come from MAR
196 model outputs. We use the common overlap period (2006-2014) to correct the bias between two
197 models outputs. The RACMO simulation was forced by the HadGEM2-ES Earth system model
198 (Collins et al., 2011), as this climate model was found to be the most realistic for present-day
199 simulations of the Greenland ice sheet (Van Angelen et al., 2013). Ocean forcing in Equations (10)
200 and (13) should relate to temperatures off the continental shelf close to the fjord mouth. Cowton et
201 al. (2018) achieved success in simulating the terminus position and yearly variability of 10 glaciers
202 along the east coast of Greenland using mean 200-400 m depth temperatures from reanalysis data.
203 For consistency with the RACMO results, we use deep ocean temperatures at ~ 300 m depth from
204 the 0.83°×1° resolution HadGEM2-ES driven by the RCP 4.5 climate scenario from 2005 to 2100
205 at the 3 closest grids point to Disko Bay. We also compare this with results from 7 other climate
206 model simulations of RCP4.5: HadGEM2-ES (Collin et al., 2011), BNU-ESM (Ji et al., 2014),
207 MIROC-ESM (Watanabe et al., 2011), IPSL-CM5A-LR (Dufresne et al., 2013), CSIRO-Mk3L-1-2
208 (Gordon et al., 2002), NorESM1-M (Bentsen et al., 2012) and MPI-ESM-LR (Giorgetta et al., 2013).

209 **2.3 Initialization Procedure**

210 As we are interested in high resolution simulations and validating our model parameterizations with
211 observations over the last decade, we take care to initialize the model as accurately as possible.
212 Detailed bedrock topography and ice thickness data in the year 2009 comes from Gogineni et al.
213 (2012); we chose the product because it has 500 m resolution and so matches the highest resolution
214 of our mesh. Jakobsson et al. (2012) provides ocean bathymetry data (Fig. 1). In 2004 the floating
215 ice shelf disintegrated, making it a convenient starting point for simulations since we might expect

216 the system to respond differently to forcing when there was a floating ice shelf compared with the
217 situation of ocean forcing along a near-vertical ice cliff. This is consistent with the observed good
218 correlation between ocean temperature and flow speed after 2004 but not before. The aim of this
219 initialization is to provide a state rather similar to 2004, that is barely retreating on inter-annual
220 scales (Joughin et al., 2010) and small changes of annual mean velocity in the following 3 years.
221 Therefore

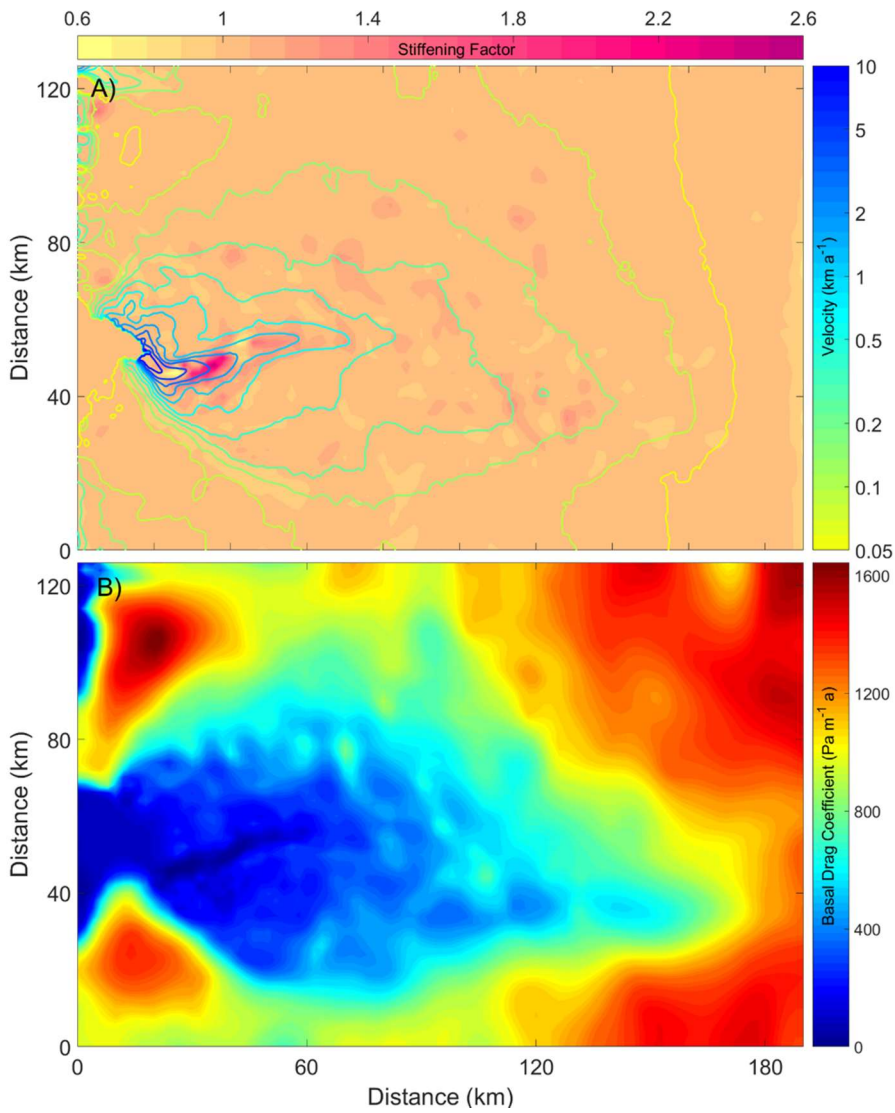
222 1) We solved the inverse problem for basal conditions (Eq. 7) and stiffening factor using 2010
223 velocities (Joughin et al., 2010) and 2009 geometry (Gogineni et al., 2012), following Cornford
224 et al. (2015). Our friction coefficient and stiffening factor fields are shown in Fig. 3. Fig. S1
225 shows the discrepancy between observed velocity field (Joughin et al., 2010) and the velocity
226 derived from the inversion.

227 2) Starting from the inversion of step 1, we let the model glacier evolve freely without calving
228 and with zero SMB and with sub-shelf melting ($\gamma=0.0238$) forced by repeating the observed
229 2004 ocean temperature for 11 years until its surface elevation profile reached a state shown in
230 Fig. S2.

231 3) We carried out several 10-year simulations each with different β values. These simulations
232 were forced by repeatedly applying the 2004 seasonal climate forcing so that the glacier
233 approaches a steady state. From these, we selected the β that provided a calving front position
234 closest to that observed in 2004. The best β here is 0.034, and this is our best guess for the 2004
235 state. The annual minimum extent of Jakobshavn retreats ~ 2 km from 2004 to 2005 following
236 the loss of ice shelf buttressing, but then stabilizes until 2007 (Joughin et al. 2010). Annual
237 maximum extents are stable over the 2004-2007 period. Front velocity increase slowly from
238 2004-2007 ($\sim 5.9\% \text{ a}^{-1}$ Joughin et al. 2010), and the model simulated velocities increase by

239 about $3\% \text{ a}^{-1}$. This period of relative stability also makes 2004 a good time from which to start
240 transient simulations.

241 Basal friction coefficient values downstream of the 2010 grounding line were set equal to that in the
242 nearest 2010 grounded location. This was necessary because steps 2 and 3 involved grounding line
243 advance beyond the region for which basal friction coefficients had been inferred. The geometry
244 after this spin up procedure, and the friction coefficient and stiffening factor distribution from the
245 inversion in step 1 were used as the initial condition for model calibration.



246

247 **Figure 3. (A) Stiffening factor Φ (Eq. 3) and (B) basal traction coefficient C (Eq. 7) over the**
248 **computational domain from solving the inverse problem. Contour lines in panel A show the**
249 **modeled velocity (logarithmic scale).**

250 **2.4 Model calibration**

251 The parameters in the model, α , β and γ representing mélange buttressing, crevasse depth sensitivity
252 to surface runoff, and shelf melt sensitivity to ocean temperatures need to be estimated. The
253 measured relationship between ocean temperatures and sub-shelf melt rate (Motyka et al., 2011)
254 gives the value of γ to be 0.238. We manually tune parameters in equations (11) and (12): α over
255 the range 0.7–1.2 for α_1 and 0.09–0.12 for α_2 ; and β (0.04 - 0.075) to best reproduce Jakobshavn
256 Isbræ's calving front position and surface velocity evolution for the 10 year period 2004–2013.
257 Reproducing the total retreat distance and the temporary stable state after 2012 were secondary
258 desirable features to match. The best set of parameters are $\alpha_1=0.82$, $\alpha_2=0.111$, $\beta=0.0638$. Since these
259 values come from a manual search we do not claim them to be the best in all parameter space. We
260 assess model sensitivity to the parameter values next.

261 We explore the glacier's sensitivity to two types of boundary perturbations. They are ice mélange
262 buttressing effect (defined by α) and submarine melting (defined by γ). We scaled submarine melt
263 rates by multiplying it by values from 0.8–1.2, based on the range of the observation uncertainty in
264 melt of $\sim 20\%$ (Motyka et al. 2011). Also we varied α by multiplying by factors from 0.91 to 1.25
265 to represent different buttressing strengths (Eq. 10). These multiplication factors were varied
266 systematically with typical intervals of 0.1 and 0.03 respectively for the γ and α factors. We
267 calculated the following relative mismatches defined as (model-observations)/observations for each
268 simulation (Fig. 4):

269 1. Total calving front retreat from 2004–2013 measured by the difference between 2004 and

270 2013's annual maximum extent.

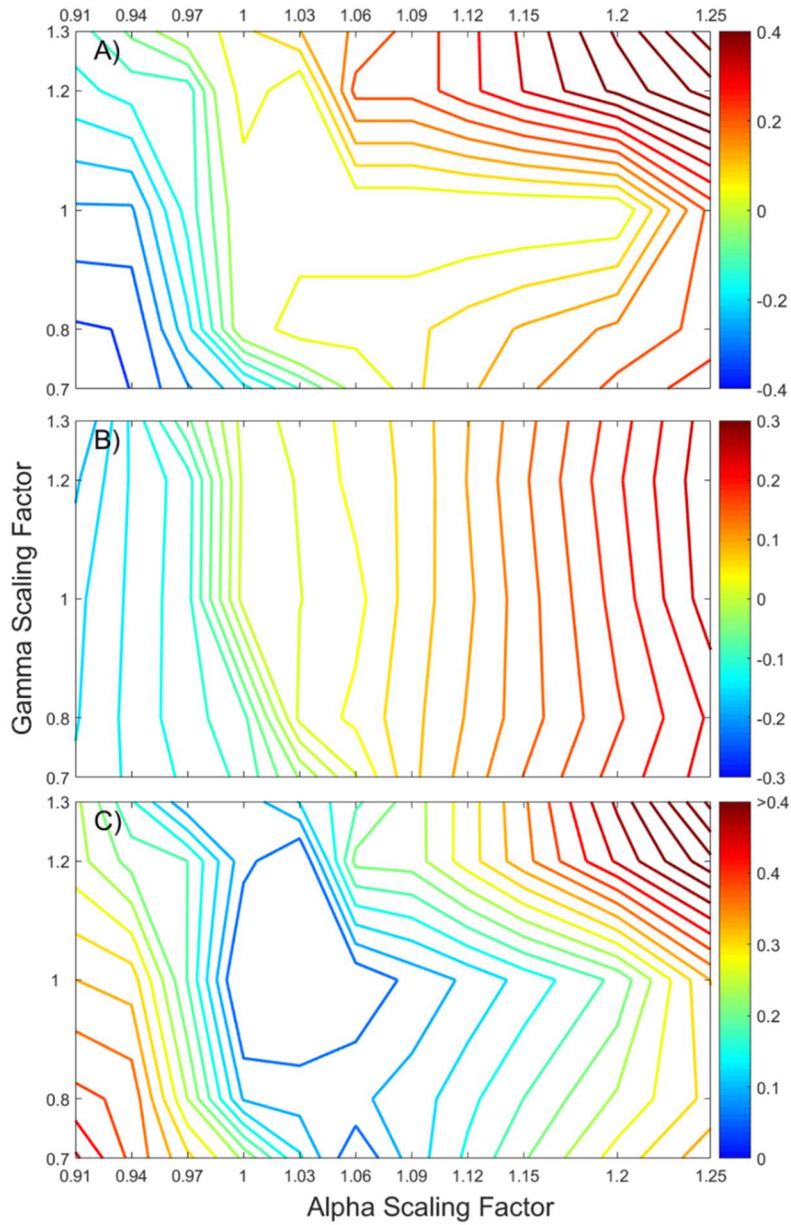
271 2. Annual mean front velocities

272 3. Vector sum of 1) and 2)

273 We used β (Eq. 12) from our optimal set of parameters. Our optimal value for α is such that a

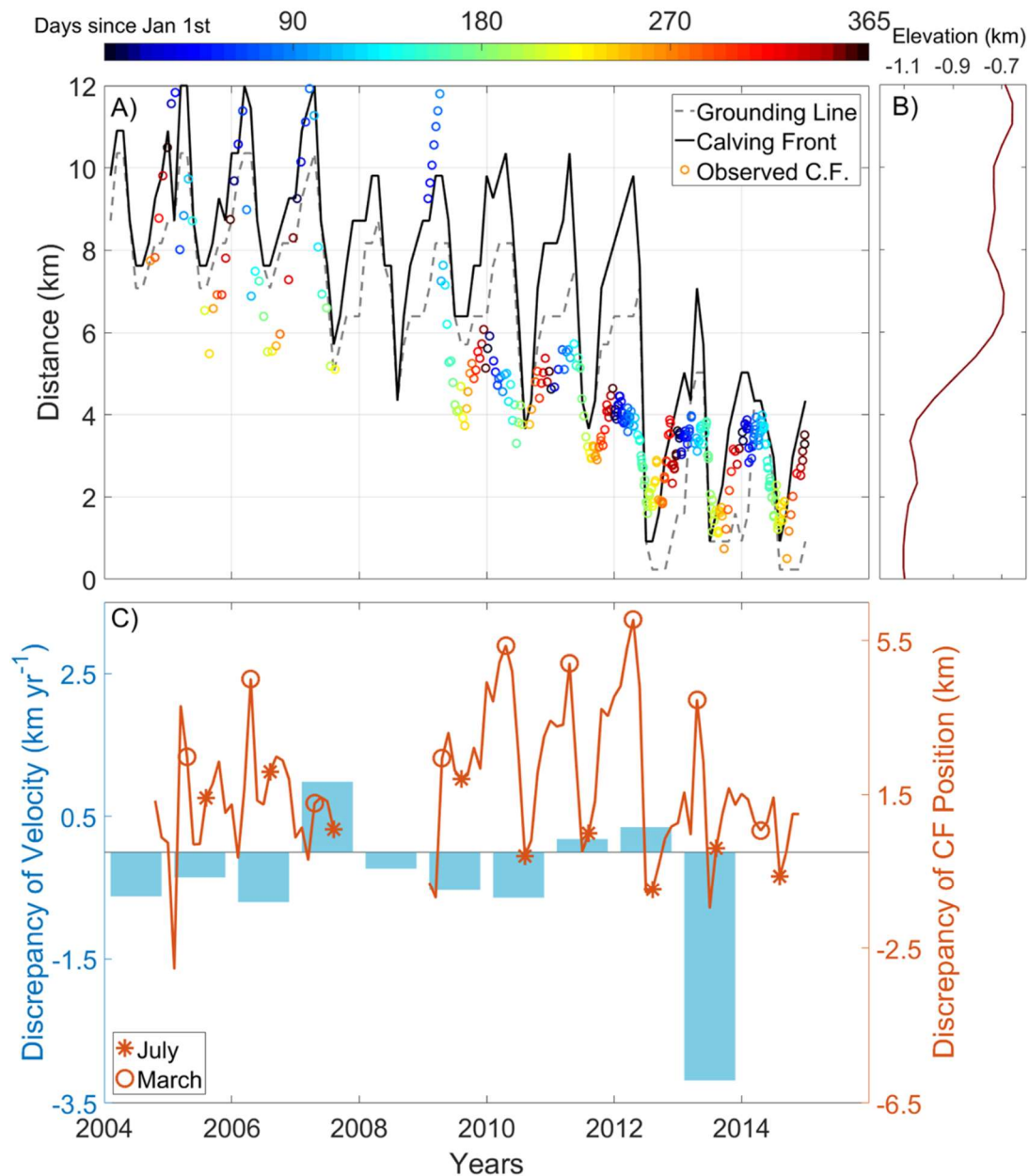
274 20% rise of its value does not affect modeled retreat when β and γ are kept to be their optimal

275 values (Fig. 4 A).



276

277 **Figure 4. Relative mismatches defined as (model-observed)/observed for A) total calving front**
 278 **retreat, B) average of annual mean front velocity during 2004-2013, C) the vector sum of**
 279 **mismatches in panels A and B, $\sqrt{A^2 + B^2}$ in our 2-D parameter space. X- and y-axis are**
 280 **multipliers of α and γ .**



281

282 **Figure 5. (A) Modeled retreat of the calving front (black solid line), grounding line (gray**
 283 **dashed line), and observed calving front positions (color-coded circles and scale bar) from**
 284 **Joughin et al. (2014). (B) Bedrock elevations. (C) Residuals (modeled minus observed) of**
 285 **annual mean front velocity (blue bars, left axis) and of calving front position (red lines, right**
 286 **axis) with typical timings of annual maximum (March) and minimum (July) extent marked.**
 287 **The modeled front velocities and calving positions explain about 49% and 76% of the variance**
 288 **in corresponding observations.**

289 The two biggest mismatches occur with the 2007 and especially 2013 velocities (Fig. 5). 2013 has
 290 the lowest simulated surface water run-off (Fig. 2) of all the years since 2004. The Benn calving

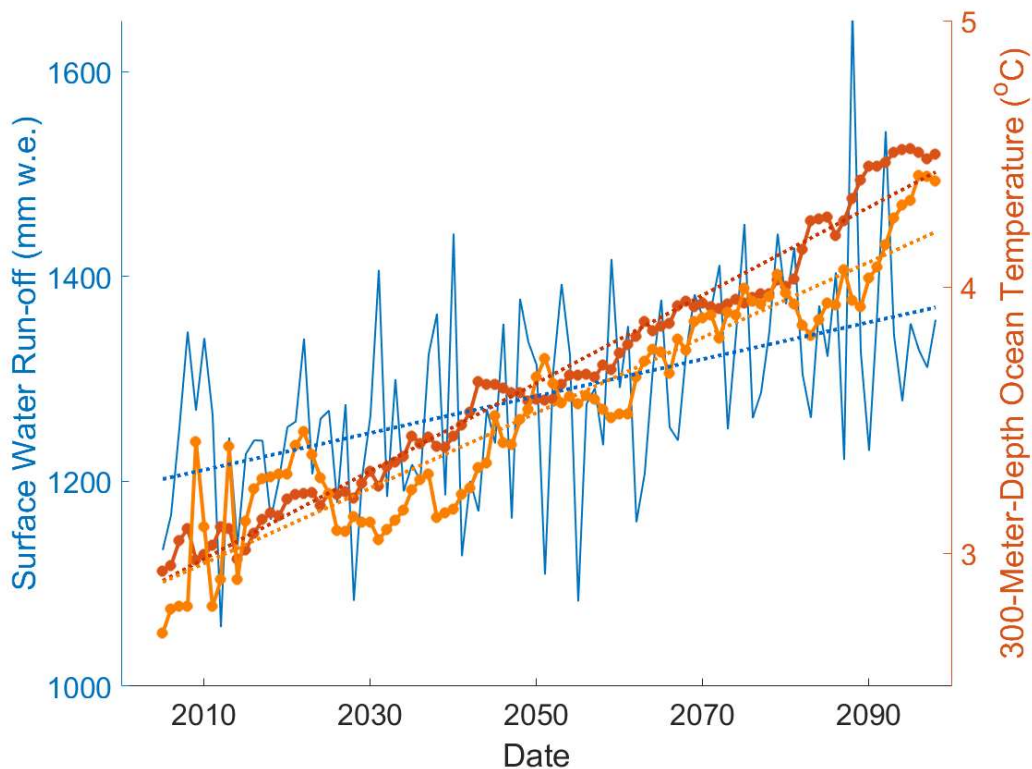
291 model we use is sensitive to runoff, with reduced run-off leading to lower crevasse-penetration-
292 depth and reduced terminus fracturing thus increasing its buttressing force. Furthermore 2013 had
293 relatively cool ocean temperatures which were lower than the average of 2004-2013. The cool ocean
294 temperatures also increased buttressing, leading to low simulated annual mean velocities.
295 Jakobshavn Isbræ did not in fact slow down very much in 2013 because there were calving events
296 (Cassotto et al. 2015) that are unrepresented in our model. The relevant mechanisms are discussed
297 later. In 2007 high run-off caused more simulated calving and retreat than in reality. These retreat
298 phases reduced the buttressing and lateral drag due to shear-margin-weakening, all of which lead to
299 excessive speed-up near the terminus.

300 Modeled calving front retreat is ~ 7 km in total from 2004-2014 (Fig. 5), which is consistent with
301 observations (Joughin et al. 2014). In 2009 a dramatic retreat brought the grounding line to the
302 bottom of the bedrock slope, and since then it has gradually retreated with smaller seasonal
303 fluctuations. The run-off forcing we applied triggered major retreats in the summers of 2007 and
304 2012, due to large summer peak run-off (Fig. 2), demonstrating the sensitivity of our calving
305 parameterization to run-off forcing. Modeled timings of maximum extent and minimum extent each
306 year are in good agreement with observations, also demonstrating that summer, in particular, May
307 to July, run-off determines much of the behavior of Jakobshavn Isbræ.

308 The modeled range of seasonal fluctuation in front position is ~ 5 km, which is similar to
309 observations in the period before 2008. From January 2009 to December 2011, there was an abrupt
310 decrease in seasonal front fluctuation, with many winter calving events occurring, in contrast with
311 previous years (Cassotto et al. 2015). These winter calving events may explain the small observed
312 seasonal fluctuations because they limit the winter advance. Our model is unable to stimulate these
313 winter calving events because there is no winter run-off, and as extension stresses are never enough

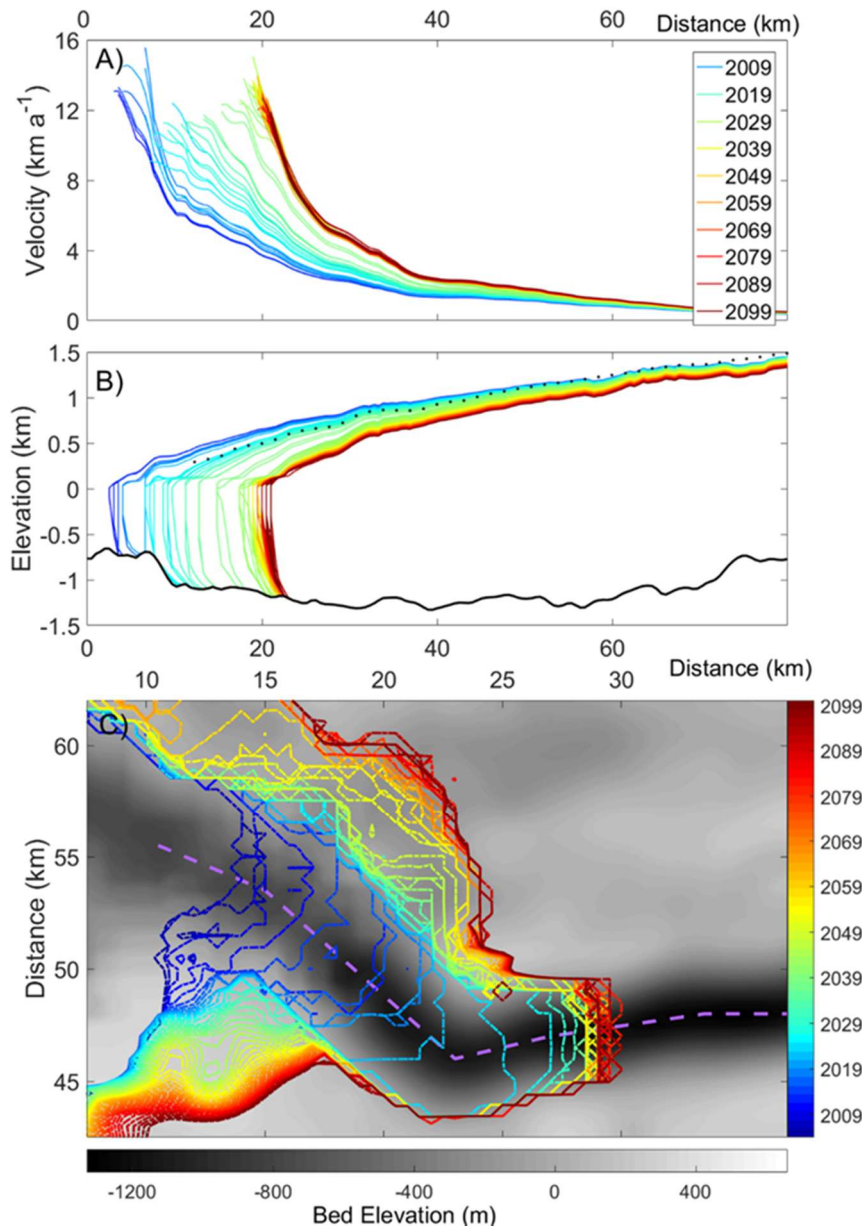
314 to cause winter calving, calving is then zero. The largest discrepancy of front position occurs during
315 these winter calving periods (Fig. 5). Observations also showed that from 2013 to 2017, Jakobshavn
316 Isbrae barely retreated (Joughin et al. 2010). The decline of run-off (Fig. 2) in 2014 suggests the
317 reason. But since no RACMO run-off simulations are yet available for 2015 and later, our
318 parameterizations cannot be tested against this lack of retreat.

319 3 Future evolution



320

321 **Figure 6. Climate forcing for future projection under the RCP4.5 scenario taken as 300 m**
322 **depth ocean temperatures from HadGEM2-ES (orange) compared with the ensemble mean**
323 **(red) of 7 Earth System Models (HadGEM2-ES, BNU-ESM, MIROC-ESM, IPSL-CM5A-LR,**
324 **CSIRO-Mk3L-1-2, NorESM1-M and MPI-ESM-LR), (right axis), with their linear trends.**
325 **Annual maximum monthly surface water run-off near Jakobshavn Isbrae’s terminus from**
326 **RACMO (forced by outputs from HadGEM2-ES) is shown in blue.**



327

328 **Figure 7. Modeled profiles of (A) January velocity and (B) January surface elevation along**
 329 **the center-flow-line (purple dash line in panel C) of Jakobshavn Isbræ from 2004 to 2099 for**
 330 **the RCP4.5 scenario. Bedrock elevation is shown in black. Black dotted line is the surface**
 331 **elevation profile extracted from radar data measured around 2010 (Gogineni et al., 2012).**
 332 **Profiles are shown at intervals of 1 years. Profiles are color-coded in the legend and range**
 333 **from blue to green and red. (C) Modeled July front positions (color bar) over its bedrock**
 334 **(grayscale bar) at intervals of 2 years.**

335 Under the RCP4.5 scenario (Fig. 6) surface runoff slowly rises over the 21st century, with RACMO

336 simulating slightly greater runoff during the second half than for the first 50 years. Runoff increases

337 by 14% over the century. Ocean temperature at 300 m depth in the grid cell closest to Jakobshavn
 338 increases by 52%, and, as may be expected, has less variability than runoff.

339 Under this forcing, Jakobshavn Isbræ continues its retreat (Fig. 7) for 18 years after 2013, producing
 340 a total grounding line retreat of ~18 km upstream. As calving produces a steepening surface profile,
 341 terminus velocities increase, to reach a 21st century peak of ~19 km a⁻¹ in 2031 summer. Eventually
 342 the front height (relative to sea level) becomes larger than the crevasse penetration depth in the
 343 calving parameterization. This leads to a stable period with little inter-annual retreat and which lasts
 344 until the end of this century. During this period, nearly all of the seasonal retreats are offset by the
 345 following winter re-advances. Mass transport continually flattens and thins the ice geometry, leading
 346 to reduced flow speeds that eventually become half those of 2031, the 21st century peak.

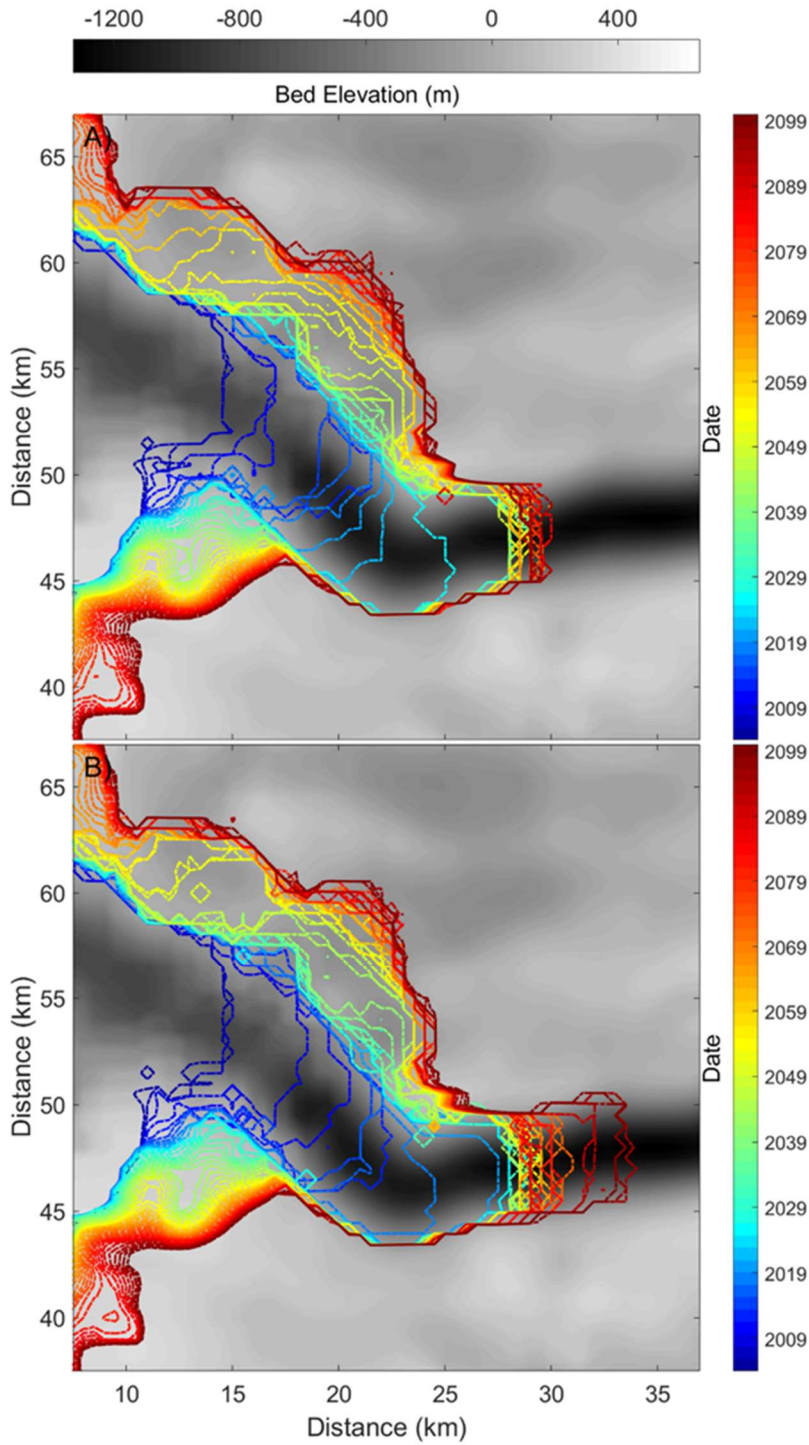
347 The surprisingly high run-off anomaly in 2088 (Fig. 6) does not affect the stable state indicating
 348 run-off fluctuation alone cannot break this retreat pattern immediately. Once the inter-annual retreats
 349 cease in 2031, the dynamic thinning rate is greatly reduced because calving front height stops
 350 increasing.

351 **Table 1 Estimates of glacier mass loss and grounding line retreat from different sources.**

Source	Climate scenario	Mass loss 2004-2013 (10 years) (Gt)	Mass loss by 2100 (Gt)	Grounding line retreat 2004-2013 (km)	Grounding line retreat by 2100 (km)
This paper	RCP4.5	234	2068 (2044-2723)	7.0	18.5 (17.5-23.0)
Muresan et al. (2016)		220			
Nick et al. (2013)	A1B		1870 - 2281		14.0 - 26.0
Observations		225 ± 15		7.0	

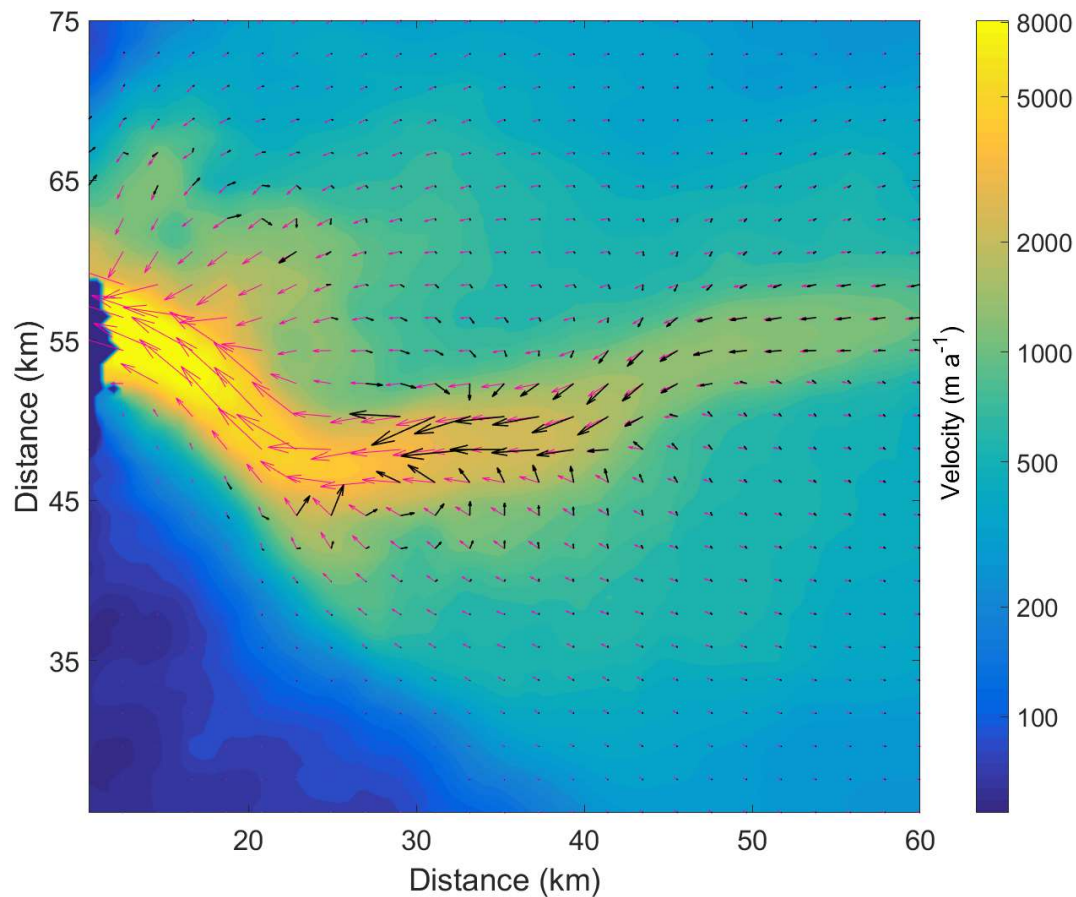
352 Table 1 shows estimates of glacier mass loss and retreat. Under RCP4.5, total cumulative mass
 353 change of Jakobshavn Isbræ is 2068 Gt by 2100, using best set of α , β and γ with ocean temperature
 354 inputs from ensemble mean of 7 ESMs (Fig. 6). To estimate an upper bound for mass loss over this

355 century, we scale the α parameter by 1.2 giving 2680 Gt for the same forcing (Fig. 8a). Using the
356 HadGEM2-ES forcing, which is the same model used to force RACMO with α and γ set to their
357 best estimates (Fig. 4) gives 2000 Gt. We suggest that this may be the lower reasonable bound of
358 mass loss since the HadGEM-ES ocean temperatures rise notably slower than the ensemble mean
359 (Fig. 6). Note that all 3 simulations of front position (Fig 7C, Fig. 8) show a relatively stable position
360 around 18 km upstream from its 2013 location. Examination of the change in velocities during the
361 simulation (Fig. 9) suggests that the explanation for this stability is strong flow convergence near
362 the future glacier front that largely offsets dynamic thinning. Notice that the South side of the fast-
363 flow-area in 20th century was quite close to ice-free land, while in later half of this century
364 convergent flow in the South is fed by a substantial area of ice stream.



365

366 **Figure 8. Upper and lower estimates of July front positions within this century with colors**
 367 **indicating the date (color bar) for A) lower bound with scalings of (1,0.8) and the HadGEM-ES**
 368 **forcing B) upper bound of mass loss projection with (α , γ) parameter scalings of (1.2,1), and the**
 369 **7-model ensemble climate forcing.**



370
 371 **Figure 9. Simulated velocity vectors in 2004 (pink vectors) with their magnitudes (right color bar)**
 372 **and velocity difference between 2004 and 2099 (2099's minus 2004's, black vectors), for clarity**
 373 **vector lengths are clipped at 5 km a⁻¹.**

374 Exploring the (α, γ) scaling parameter space we notice that values of (1.0, 0.8) produce a mass loss
 375 over this century of 2021 Gt with the HadGEM-ES ocean forcing, almost the same value as for the
 376 best set of parameters. This implies that less submarine melting (determined by γ) leads to larger ice
 377 loss by dynamic processes. The reason is that lesser submarine melt allows a larger ice thickness at
 378 the grounding line with stronger dynamic thinning in advancing season. Notice in our stress balance
 379 equation (Eq. 3), thickness contributes to driving force term, thus ice flux across the grounding line
 380 is highly nonlinear in ice thickness. This highly nonlinear relationship is also shown in our
 381 sensitivity tests (Fig. 4). Over the mismatch field measured by front velocity (Fig. 4, Panel B), the
 382 velocity is partly dominated by low values of γ scaling around the scaling line for $\alpha = 1.06$, while α

383 is almost the only control on velocity over the region where scaled $\alpha < 1.09$. Within our sample space,
384 the non-linear and non-monotonic relationship between submarine melting and retreats is clear (Fig.
385 4, Panel A). Around the point of scalings ($\alpha = 1.12$, $\gamma = 1.0$), total retreat will increase no matter if γ
386 is decreasing or increasing within the scaling range $0.8 < \gamma < 1.2$. The area where scaled $\alpha > 1.0$ in
387 sample space is the very likely future condition for Jakobshavn Isbræ because increasing terminal
388 ice cliff height caused by retreating into deep water will act as an amplifier to frontal driving force.

389 **4 Discussion**

390 **4.1 Parameterization of Buttressing effect**

391 The sudden 1.1°C rise in temperature of water entering Ilulissat fjord in 1997 (Holland et al., 2008)
392 initiated rapid melting and disintegration of the ice shelf in 2003. This disintegration coincided with
393 a near doubling of ice velocities. Modeling (Vielé et al., 2011) suggested that this was due to the
394 reduction in buttressing from the ice-mélange. We can realistically reproduce the velocity variation
395 of Jakobshavn Isbræ on seasonal and inter-annual scales using our parameterization of the
396 buttressing effect from the ice mélange in the fjord.

397 Gladish et al. (2015) analyzed glacial flow speeds from 1998 to 2014, finding no correlation with
398 Ilulissat fjord temperatures. This is because at the beginning of 2004, Jakobshavn's evolution entered
399 a new phase with the disintegration of the ice shelf. We find good correlations between Disko Bay
400 temperatures and ice velocities from 2004 to 2014. The improvement in correlation with
401 temperatures may be explained by a faster response between the grounded glacier and the fjord
402 water temperatures after loss of the floating ice shelf.

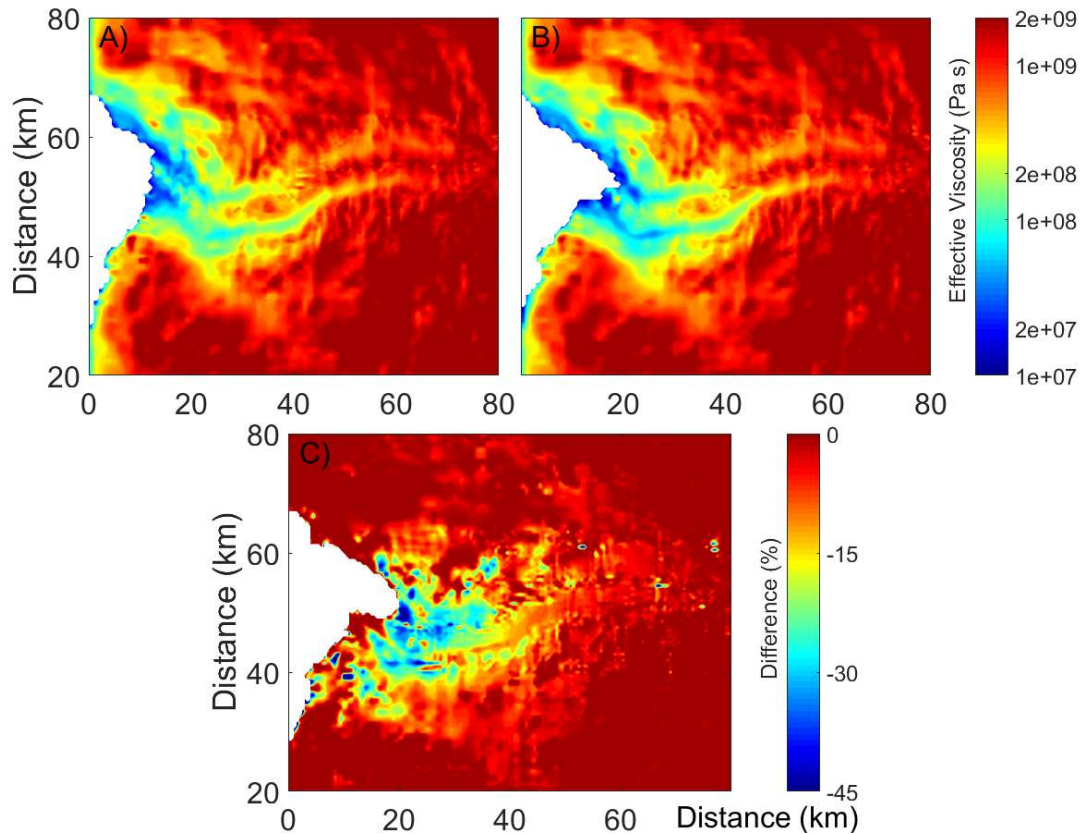
403 Buttressing would affect the calving process by altering the longitudinal resistive stress in the glacier.

404 Temperatures in Ilulissat Fjord will be warmer during the 21st century under essentially all climate
405 scenarios, even those with modest emissions, due to the thermal inertia of the oceans. Thus a new
406 floating ice shelf is unlikely to form. Prior to 2004, there were large changes in Jakobshavn: loss of
407 ~15 km long ice shelf and the sudden rise in fjord temperatures in 1998. There are fewer mechanisms
408 to effect such dramatic changes in the future now that almost the entirety of the glacier is grounded.
409 We therefore propose that our representation of the *mélange* buttressing mechanism, tuned for 2004-
410 2013, is likely to maintain its validity during the 21st century.

411 **4.2 Horizontal shearing and viscosity**

412 Van Der Veen et al. (2011) estimated a maximum horizontal shear stress of ~800 kPa across the
413 shear margin of Jakobshavn Isbræ where the horizontal velocity shear reaches the peak, while the
414 bed stress is only 10-40 kPa in fast flowing regions (Shapiro et al., 2016). Given that the width of
415 the Jakobshavn Isbræ fast flow region is typically under 5 km and its thickness is typically between
416 1-2 km, these numbers indicate that the shear margins provide at least an order of magnitude greater
417 total resistance than the bed. Thus, the shear margin, rather than the bed of Jakobshavn Isbræ
418 provides most of the resistance balancing the driving force. The main trunk of Jakobshavn Isbræ
419 exhibits considerable seasonal velocity changes, while the slow moving ice outside the shear margin
420 has little or no seasonal cycle. This flow structure implies speed gradients perpendicular to the flow
421 direction with large seasonal variation. These velocity shears would in turn generate large seasonal
422 variations in effective ice viscosity (Eq. 6). This mechanism is due to the non-linear rheology of the
423 ice in the fast flow region: increases in the speed of fast flowing ice cause increases in horizontal
424 shear stress across the margins, reduced viscosity, and further increased horizontal velocity shear,
425 allowing further increase to speeds in the fast flow region. Observations show that, as the terminus
426 retreated into deeper water, seasonal fluctuations in terminus velocity increased (Joughin et al. 2008).

427 By 2012, the summer time peak terminus velocity was $\sim 17 \text{ km a}^{-1}$, more than twice the wintertime
 428 minimum velocity (Joughin et al. 2014). This amplified seasonal velocity cycle was likely enhanced
 429 by the shear-margin weakening mechanism.



430

431 **Figure 10. Modeled annual mean of vertically averaged effective viscosity $\Phi\mu$ (Eq. 5) in 2004**
 432 **(A) and 2013 (B) and the percentage decreases from 2004 to 2013 (C).**

433 Our modeled shear margin weakening on decadal scales is consistent with other estimates from a
 434 thermomechanical ice flow model of Jakobshavn Isbræ forced by calving front positions (Bondzio
 435 et al., 2017). Their modeled viscosity drops between 2003 to 2015 reach $\sim 40\%$ which is close to
 436 our maximum viscosity decrease of $\sim 45\%$ between 2004 to 2013 (Fig. 10). The extreme calving
 437 season we simulated in summer 2012 was accompanied by $\sim 12 \text{ km a}^{-1}$ variations in speed at the
 438 calving front, which were facilitated by the accompanying shear margin-induced ice viscosity

439 reductions of 60% at the time of maximum terminus advance. Simpler models of Jakobshavn Isbræ,
440 using a flowband model (Nick et al., 2013) or simple calving parameterizations with no seasonal
441 cycle (Muresan et al., 2016) cannot produce these seasonal variations in shearing. However, our
442 model accommodates both the seasonal forcing from calving and the three-dimensional seasonal
443 velocity shear impacts on effective viscosity. Without this physical process, speedups during intense
444 calving events would be under-estimated, and this would lead to under-estimated mass
445 transportation during the retreat. Bondzio et al. (2017) used a thermomechanical ice flow model to
446 evolve the ice viscosity, which depends on a damage parameter that softens the ice in the shear
447 margins. But their damage parameter also stays constant in time. Thus both the models of Bondzio
448 et al., (2017) and ours only consider the contribution from strain rate weakening in time to evolving
449 viscosity. Thermodynamics could play some role in changing viscosity, presumably if the ice
450 temperatures increased over time, but our temperatures are fixed at -10°C .

451 Several processes absent from our model could affect ice viscosity. Crevasses saturated by surface
452 melt water within the shear margins of Jakobshavn are visible on satellite images (Lampkin et al.,
453 2013). This melt water can transfer heat throughout the ice column through discharge within
454 crevasses and moulins thus softening the ice (Phillips et al., 2010). Incorporating a continuum
455 damage model in BISICLES would further exaggerate the shear margin weakening as it raises the
456 non-linear dependence of strain rates on stress fields (Sun et al., 2017).

457 **4.3 Comparison with previous estimates**

458 The cumulative mass change of Jakobshavn Isbræ estimated from airborne and satellite laser
459 altimetry for 1997–2014 was tabulated Muresan et al. (2016). The mass loss over the 10-year period
460 2004–2013 modeled by Muresan et al. (2016) is closer to observations than ours (Table 1). This is
461 partly due to different tuning targets: matching observed mass change was a stated target in their

462 study, whereas our study targets ice front position and velocity. Their close match to observed mass
463 loss may be partly due to cancelling errors: 1) their modeled calving front barely moves after 2006,
464 which leads to under-estimation of mass change; and 2) the modeled fast flow widths are larger than
465 observations, which amplifies the mass flux across the calving front. These two biases will not
466 always offset each other perfectly in the future.

467 Muresan et al. (2016) failed to simulate the retreat of Jakobshavn Isbræ after 2010. This may be due
468 to the thickness threshold employed in their calving parameterization. Once Jakobshavn Isbræ
469 terminus has retreated into the deeper part of the bedrock trough, the terminus height might never
470 drop below their calving threshold of 375 m. In this case their calving rate will be solely due to the
471 eigen parameterization of strain rates. Moreover, absence of seasonality in their calving front leads
472 to under-estimated dynamic thinning, which is a key prerequisite for further calving. In contrast,
473 our crevasse-depth calving model depends on stresses and surface water run-off with strong seasonal
474 variation. As the terminus retreats and the surface slope steepens the enhanced surface stretching
475 enhances the opening of crevasses in both calving parameterizations.

476 Nick et al. (2013) used a flow-band model to estimate a mass loss of 2280 Gt for Jakobshavn Isbræ
477 by 2100 under the A1B climate scenario (Table 1). In our model we use RCP4.5 climate forcing,
478 which has lower temperature rises than A1B, especially after 2050. Nick et al. (2013) prescribed a
479 flow-band that has a near uniform width of 5 km near the terminus. Later modeling work using a
480 similar model suggested that stability of the glacier is fundamentally controlled by geometry, and in
481 reality the width varies along the ice-stream (Steiger et al. 2017). Nick et al. (2013) chose sets of
482 parameters that produced small inter-annual retreats of Jakobshavn from 2000-2010, which may
483 limit mass loss and retreat. The absence of the shear margin weakening feedback in their model also
484 likely causes underestimation of mass loss. This could account for the comparable projected mass

485 loss to our results, and less terminus retreat (Table 1), even though their climate forcing scenario
486 was warmer.

487 Another SSA model (Bondzio et al., 2018) projects larger retreats than ours, and uses a calving
488 parameterization that predicts the location of calving depending on tensile stress distribution,
489 regardless of ice thickness. In contrast our calving parameterization uses mélange buttressing effects
490 and calving driven by seasonal filling of crevasses with surface water run-off, while Bondzio et al.
491 (2018) drive their calving seasonality by a seasonal varying stress threshold. However, in the real
492 world Jakobshavn, calving does not have to be of the full-thickness-type and can involve vertical
493 motions (Xie et al., 2016) or the MICI (Marine Ice Cliff Instability) mechanism (Pollard et al., 2015),
494 all of which are difficult to resolve by an SSA model. These calving types are probably becoming
495 more and more important as it retreats into deep water. Therefore, we cannot confidently claim our
496 crevasse-depth based calving parameterization is better than the calving criterion that only depends
497 on tensile stress (Bondzio et al., 2018) for the future. In the next section we discuss how the model
498 might be improved.

499 **4.4 Model improvements**

500 We overestimate mass loss relative to observations over Jakobshavn Isbræ drainage basin for 2004-
501 2013 (Table 1). One reason for the discrepancy may be errors in initial ice thickness and real
502 geometry in 2004. Excessive dynamic thinning was simulated over the lowest ~ 20 km of the main
503 trunk due to over-estimated summer speed. For example, modeled front velocity soared to a peak
504 of ~ 20 km a⁻¹ in summer 2012, while the observed maximum speed is only 18 km a⁻¹ (Joughin et
505 al., 2014). In this summer, we simulated a series of full-thickness calving events that eventually left
506 an unprecedented tall ice cliff. In reality, calving events do not always occur to full thickness, thus
507 the glacier tends to form a shorter ice cliff that caters for lower velocity and less dynamic thinning.

508 Since the grounding line of Jakobshavn retreated to the bottom of a reverse bed slope in 2009, the
509 height of the calving front has generally increased, causing larger mass flux downstream across the
510 calving front. Instead of enhancing the seasonal fluctuation of calving front position, substantial
511 winter calving events have occurred instead. Given the fact that these calving events have reduced
512 the typical winter advance from ~ 6 km to ~ 3 km since 2010, winter calving is now likely as
513 important as summer run-off-driven calving. During this period of low magnitude seasonal
514 fluctuations, a series of retreats gradually moved the calving front position on inter-annual scale. In
515 contrast, the inter-annual retreats before 2009 were mostly driven by single calving seasons, e.g.,
516 May to July 2009. Our model using the Benn calving model is better able to simulate this earlier
517 retreat pattern, which is largely determined by each year's peak surface water run-off.

518 The grounding line of Jakobshavn Isbræ is unlikely to return to shallow water in the remainder of
519 the 21st century because bedrock elevations < -1000 m beneath the main trunk further extend ~ 60
520 km inland. Accordingly, the latest retreat pattern including winter calving, is likely closer to the
521 pattern of future evolution of Jakobshavn Isbræ. A short floating part due to winter calving is always
522 accompanied by weaker lateral drag and steeper surface slope near the grounding line, all of which
523 are conducive for faster ice-flow. So, winter calving would enhance the downstream mass
524 transportation, a missing process in our model.

525 The process of winter calving must take place without any surface water. That calving must be
526 generated by processes affecting ice front stability, and that is likely due to changes at the base rather
527 than the surface. Evidence of calving by opening of basal crevasses and splitting comes from
528 terrestrial radar showing the terminus lifting several days prior to a large calving (Xie et al., 2016;
529 James et al., 2014). These observations suggest that the glacier is not in hydrostatic equilibrium
530 during calving. Our simulation specifies the glacier is in hydrostatic equilibrium on timescales of

531 the simulation. Our model cannot simulate the process of up-lifting. Instead we assume the upper
532 and lower surface would instantly lift to the state of floating (Eq. 1). However, there is some
533 evidence that Jakobshavn must behave super-buoyantly in winter. We observe that the simulated
534 grounding line of Jakobshavn retreats even after cessation of calving front retreat (Fig. 3). These
535 retreats can be explained by rapid dynamic thinning near the grounding line leading to its buoyancy
536 exceeding gravity and, consequently, floating. Winter calving can occur in later winter (Cassotto et
537 al., 2015) when calving front height is at its annual minimum and presumably at its least vulnerable
538 to structural failure. Hence, MICI cannot explain this type of calving (Pollard et al., 2015). The
539 existence of winter calving has greatly reduced the range of seasonal fluctuations in front position,
540 which inhibited the growing of a temporary ice shelf that would buttress the grounded ice. Thus,
541 lack of winter calving would cause underestimation of dynamic thinning as the glacier grows in
542 winter.

543 A combination of discrete element model and continuum ice-dynamic model (solving the 3-
544 Dimensional full-stokes equation) is able to reliably replicate observed calving styles in the case of
545 a super-buoyant terminus (Benn et al. 2017). The discrete element model allows investigation of
546 calving processes in unprecedented detail by analyzing the stress pattern dominated by glacier
547 geometry and boundary conditions. However, these calving processes are beyond the capability of
548 a calving parameterization based on surface crevasse depth assuming depth-independent flow.
549 Better understanding of this buoyancy-driven calving and further model development to represent
550 more details such as fracture propagation are needed to accurately simulate glacier's future
551 evolution.

552 Ice thickness and basal topography with resolution of 150 m became available for main outlet
553 glaciers of Greenland (Morlighem et al., 2017) recently (Fig. S3). This eases finer mesh resolution

554 to be used for modeling which then might reveal more details of ice-stream behavior especially
555 perpendicular-to-flow direction, including more precise shear-margin-weakening and calving near
556 side walls. Our assumption of simple Weertman basal drag (Eq. 7) may be improved by
557 implementing a physics-based basal sliding law (Schoof, 2010; Gagliardini et al., 2014; Tsai et al.,
558 2015), although basal drag accounts for only about 2% of present-day buttressing (Shapiro et al.,
559 2016). An improved sliding relation would likely produce more speedup and retreats in model
560 results as dynamic thinning can reduce the effective pressure, leading to lower basal shear stress.

561 **5 Conclusion**

562 We use a three-dimensional dynamic ice-sheet model with a physically-based calving
563 parameterization to model the evolution of Jakobshavn Isbræ. After tuning the parameters, our
564 model can accurately reproduce Jakobshavn Isbræ's retreats and velocity changes from 2004-2013
565 on both seasonal and inter-annual scale. We project Jakobshavn Isbræ's future dynamic changes
566 with climate forcing data from RACMO (2014-2099) and an ensemble mean of 7 Earth System
567 Models for the RCP4.5 scenario.

568 We successfully model two-dimensional ice velocity and viscosity structures and their seasonal
569 variations for Jakobshavn Isbræ, which are missing from several previous modeling studies.
570 Moreover, capturing these two-dimensional structures allows us to handle the influence of
571 horizontal velocity shear on effective ice viscosity, which impacts on speedup processes of
572 Jakobshavn Isbræ.

573 We predict that Jakobshavn Isbræ's grounding line will retreat along the deep parts of a basal trough
574 where bedrock elevation is significantly lower than at the present grounding line until about 2070.
575 Retreat slows as the front reaches the deepest parts of the trough, but by the end of the century

576 acceleration is possible as the front passes that position. Using the current generation of calving
577 parameterizations, which are essentially thickness threshold models, is challenging because of the
578 increasing height of the calving front as Jakobshavn Isbræ retreats, meaning that crevasse
579 penetration depths become too small to initiate calving. Our model successfully reproduced
580 Jakobshavn Isbræ's retreat down a reverse bed slope with an elevation drop of ~ 400 m and the
581 subsequent temporarily stable calving front position in 2013 and 2014.

582 Our results suggest that rapid dynamic thinning and calving caused by deep crevasse penetration
583 are responsible for most of its recent mass loss, and will be decisive processes in future mass loss.
584 Further exploration of the physics of calving and basal sliding of Greenland outlet glaciers are
585 required to improve future projections.

586 *Code and data availability.* All data sets used are publicly available as listed in references. All scripts
587 used for simulations and post-treatment as well as model output are available upon request from
588 authors.

589 *Competing interests.* The authors declare that they have no conflict of interest.

590 *Acknowledgements.* This study is supported by National Key Research and Development Program
591 of China (2018YFC1406104), National Key Science Program for Global Change Research
592 (2015CB953601) and National Natural Science Foundation of China (No. 41506212). We thank
593 Stephen Cornford for his help in implementing some parameterizations used in our model. Three
594 referees provided very helpful suggestions on the model results. Rupert Gladstone is supported by
595 Academy of Finland grant number 286587.

596 **References**

597 Alexander, P. M., and Luthcke, S. B.: Greenland Ice Sheet seasonal and spatial mass variability from
598 model simulations and GRACE (2003-2012), *The Cryosphere*, 10(3), 1259, 2016.

599 Amundson, J. M., Fahnestock, M., Truffer, M., Brown, J., Lüthi, M. P., and Motyka, R. J.: Ice
600 mélange dynamics and implications for terminus stability, Jakobshavn Isbræ, Greenland, *J. Geophys.*

- 601 Res.-Earth Surf., 115(F1), 2010.
- 602 Bamber, J. L., Layberry, R. L., and Gogineni, S. P.: A new ice thickness and bed data set for the
603 Greenland ice sheet: 1. Measurement, data reduction, and errors, *J. Geophys Res.-Atmos*, 106(D24),
604 33773-33780, 2001.
- 605 Benn, D. I., Åström, J., Zwinger, T., Todd, J., Nick, F. M., Cook, S., Hulton, N. R.J., and Luckman,
606 A.: Melt-under-cutting and buoyancy-driven calving from tidewater glaciers: new insights from
607 discrete element and continuum model simulations, *J. Glaciol.*, 63(240), 691-702, 2017.
- 608 Benn, D. I., Warren, C. R., and Mottram, R. H.: Calving processes and the dynamics of calving
609 glaciers, *Earth-Sci Rev.*, 82(3), 143-179, 2007.
- 610 Bentsen, M., Bethke, I., Debernard, J. B., Iversen, T., Kirkevåg, A., Seland, Ø., Drange, H., Roelandt,
611 C., Seierstad, I. A., Hoose, C., and Kristjánsson, J. E.: The Norwegian earth system model,
612 NorESM1-M-Part 1: Description and basic evaluation, *Geosci. Model Dev.*, 5, 2843-2931, 2012.
- 613 Block, A. E., and Bell, R. E.: Geophysical evidence for soft bed sliding at Jakobshavn Isbrae, West
614 Greenland, *The Cryosphere Discussions*, 5, 339-366, 2011.
- 615 Bondzio, J. H., Morlighem, M., Seroussi, H., Kleiner, T., Rückamp, M., Mouginot, J., Moon, T.,
616 Larour, E. Y., and Humbert, A.: The mechanisms behind Jakobshavn Isbræ's acceleration and mass
617 loss: A 3-D thermomechanical model study, *Geophys. Res. Lett.*, 44(12), 6252-6260, 2017.
- 618 Bondzio, J. H., Morlighem, M., Seroussi, H., Wood, M. H., and Mouginot, J.: Control of ocean
619 temperature on Jakobshavn Isbræ's present and future mass loss, *Geophys. Res. Lett.*, 45(23), 12-
620 912, 2018.
- 621 Cassotto, R., Fahnestock, M., Amundson, J. M., Truffer, M., and Joughin, I.: Seasonal and
622 interannual variations in ice mélange and its impact on terminus stability, Jakobshavn Isbrae,
623 Greenland, *J. Glaciol.*, 61(225), 76-88, 2015.
- 624 Collins, W. J., Bellouin, N., Doutriaux-Boucher, M., Gedney, N., Halloran, P., Hinton, T., Hughes,
625 J., Jones, C. D., Joshi, M., Liddicoat, S., Martin, G., O'Connor, F., Rae, J., Senior, C., Sitch, S.,
626 Totterdell, I., Wiltshire, A., and Martin, G.: Development and evaluation of an Earth-System model
627 HadGEM2, *Geosci. Model Dev.*, 4(4), 1051-1075, 2011.
- 628 Cornford, S. L., Martin, D. F., Graves, D. T., Ranken, D. F., Le Brocq, A. M., Gladstone, R. M.,
629 Payne, A. J., Ng, E. G., and Lipscomb, W. H.: Adaptive mesh, finite volume modeling of marine
630 ice sheets, *J. Comput. Phys.*, 232(1), 529-549, 2013.
- 631 Cornford, S. L., Martin, D. F., Payne, A. J., Ng, E. G., Le Brocq, A. M., Gladstone, R. M., Edwards,
632 T. L., Shannon, S. R., Agosta, C., Van Den Broeke, M. R., Hellmer, H. H., Krinner, G., Ligtenberg,
633 S. R. M., Timmermann, R., and Hellmer, H. H.: Century-scale simulations of the response of the
634 West Antarctic Ice Sheet to a warming climate, *The Cryosphere*, 9, 1-22, 2015.
- 635 Cowton, T. R., Sole, A. J., Nienow, P. W., Slater, D. A., and Christoffersen, P.: Linear response of
636 east Greenland's tidewater glaciers to ocean/atmosphere warming, *P. Natl. Acad. Sci. USA*, 115(31),
637 7907-7912, 2018.
- 638 Csatho, B., Schenk, T., Van Der Veen, C. J., and Krabill, W. B.: Intermittent thinning of Jakobshavn
639 Isbrae, West Greenland, since the little ice age, *J. Glaciol.*, 54(184), 131-144, 2008.

- 640 Cuffey, K. M., and Paterson, W. S. B.: The physics of glaciers. Academic Press, 2010.
- 641 Dee, D., Uppala, S., Simmons, A., Berrisford, P., Poli, P., Kobayashi, S., Andrae, U., Balmaseda,
642 M., Balsamo, G., Bauer, P., Bechtold, P., Beljaars, A. C. M., van de Berg, L., Bidlot, J., Bormann,
643 N., Delsol, C., Dragani, R., Fuentes, M., Geer, A. J., Haimberger, L., Healy, S. B., Hersbach, H.,
644 Hólm, E. V., Isaksen, I., Kållberg, P., Köhler, M., Matricardi, M., McNally, A. P., Monge-Sanz, B.
645 M., Morcrette, J. J., Park, B. K., Peubey, C., de Rosnay, P., Tavolato, C., Thépaut, J. N., and Vitart,
646 F.: The ERA-Interim reanalysis: Configuration and performance of the data assimilation system, Q.
647 J. Roy. Meteor. Soc., 137, 553–597, 2011.
- 648 Dufresne, J. L., Foujols, M. A., Denvil, S., Caubel, A., Marti, O., Aumont, O., Balkanski, Y., Bekki,
649 S., Bellenger, H., Benschila, R., Bony, S., Bopp, L., Braconnot, P., Brockmann, P., Cadule, P., Cheruy,
650 F., Codron, F., Cozic, A., Cugnet, D., De Noblet, N., Duvel, J. P., Eth'è, C., Fairhead, L., Fichefet,
651 T., Flavoni, S., Friedlingstein, P., Grandpeix, J. Y., Guez, L., Guilyardi, E., Hauglustaine, D.,
652 Hourdin, F., Idelkadi, A., Ghattas, J., Joussaume, S., Kageyama, M., Krinner, G., Labetoulle, S.,
653 Lahellec, A., Lefebvre, M. P., Lefevre, F., Levy, C., Li, Z. X., Lloyd, J., Lott, F., Madec, G., Mancip,
654 M., Marchand, M., Masson, S., Meurdesoif, Y., Mignot, J., Musat, I., Parouty, S., Polcher, J., Rio,
655 C., Schulz, M., Swingedouw, D., Szopa, S., Talandier, C., Terray, P., Viovy, N., and Bony, S.:
656 Climate change projections using the IPSL-CM5 Earth System Model: from CMIP3 to CMIP5,
657 Clim. Dynam., 40(9-10), 2123-2165, 2013.
- 658 Gagliardini, O., Passalacqua, O., and Werder, M. A.: Retroactions between Basal Hydrology and
659 Basal Sliding from Numerical Experiments. In AGU Fall Meeting Abstracts, 2014.
- 660 Giorgetta, M. A., Jungclaus, J., Reick, C. H., Legutke, S., Bader, J., Böttinger, M., Brovkin, V.,
661 Crueger, T., Esch, M., Fieg, K., Glushak, K., Gayler, V., Haak, H., Hollweg, H., Ilyina, T., Kinne,
662 S., Kornbluh, L., Matei, D., Mauritsen, T., Mikolajewicz, U., Mueller, W., Notz, D., Pithan, F.,
663 Raddatz, T., Rast, S., Redler, R., Roeckner, E., Schmidt, H., Schnur, R., Segschneider, J., Six,
664 Katharina D., Stockhause, M., Timmreck, C., Wegner, J., Widmann, H., Wieners, K., Claussen, M.,
665 Marotzke, J., Stevens, B., and Glushak, K.: Climate and carbon cycle changes from 1850 to 2100
666 in MPI-ESM simulations for the Coupled Model Intercomparison Project phase 5, J. Adv. Model
667 Earth Sy., 5(3), 572-597, 2013.
- 668 Gladish, C. V., Holland, D. M., Rosing-Asvid, A., Behrens, J. W., and Boje, J.: Oceanic boundary
669 conditions for Jakobshavn Glacier. Part I: Variability and renewal of Ilulissat Icefjord waters, 2001-
670 14, J. Phys. Oceanogr., 45(1), 3-32, 2015.
- 671 Gogineni, P.: CReSIS radar depth sounder data, Center for Remote Sensing of Ice Sheets, Lawrence,
672 KS <https://data.cresis.ku.edu>, 2012.
- 673 Gordon, H. B., Rotstayn, L. D., McGregor, J. L., Dix, M. R., Kowalczyk, E. A., O'Farrell, S. P.,
674 Waterman, L. J., Hirst, A. C., Wilson, S. G., Collier, M. A., and Watterson, I. G.: The CSIRO Mk3
675 climate system model, 2002.
- 676 Habermann, M., Truffer, M., and Maxwell, D.: Changing basal conditions during the speed-up of
677 Jakobshavn Isbræ, Greenland, The Cryosphere, 7(6), 1679-1692, 2013.
- 678 Holland, D. M., Thomas, R. H., De Young, B., Ribergaard, M. H., and Lyberth, B.: Acceleration of
679 Jakobshavn Isbrae triggered by warm subsurface ocean waters, Nat. Geosci., 1(10), 659, 2008.
- 680 Howat, I. M., Ahn, Y., Joughin, I., van den Broeke, M. R., Lenaerts, J. T., and Smith, B.: Mass
681 balance of Greenland's three largest outlet glaciers, 2000-2010, Geophys. Res. Lett., 38(12), 2011.

- 682 Jakobsson, M., Mayer, L., Coakley, B., Dowdeswell, J. A., Forbes, S., Fridman, B., Hodnesdal, H.,
683 Noormets, R., Pedersen, R., Rebesco, M., Schenke, H. W., Zarayskaya, Y., Accettella, D.,
684 Armstrong, A., Anderson, R. M., Bienhoff, P., Camerlenghi, A., Church, I., Edwards, M., Gardner,
685 J. V., Hall, J. K., Hell, B., Hestvik, O., Kristoffersen, Y., Marcussen, C., Mohammad, R., Mosher,
686 D., Nghiem, S. V., Pedrosa, M. T., Travaglini, P. G., and Schenke, H. W.: The international
687 bathymetric chart of the Arctic Ocean (IBCAO) version 3.0, *Geophys. Res. Lett.*, 39(12), 2012.
- 688 James, T. D., Murray, T., Selmes, N., Scharrer, K., and O’Leary, M.: Buoyant flexure and basal
689 crevassing in dynamic mass loss at Helheim Glacier, *Nat. Geosci.*, 7(8), 593-596, 2014.
- 690 Ji, D., Wang, L., Feng, J., Wu, Q., Cheng, H., Zhang, Q., Yang, J., Dong, W., Dai, Y., Gong, D.,
691 Zhang, R., Wang, X., Liu, J., Moore, J. C., Chen, D., and Zhang, R. H.: Description and basic
692 evaluation of Beijing Normal University Earth system model (BNU-ESM) version 1, *Geosci. Model
693 Dev.*, 7(5), 2039-2064, 2014.
- 694 Joughin, I., Abdalati, W., and Fahnestock, M.: Large fluctuations in speed on Greenland’s
695 Jakobshavn Isbrae glacier, *Nature*, 432(7017), 608, 2004.
- 696 Joughin, I., Howat, I. M., Fahnestock, M., Smith, B., Krabill, W., Alley, R. B., Stern, H., and Truffer,
697 M.: Continued evolution of Jakobshavn Isbrae following its rapid speedup, *J. Geophys. Res.-Earth
698 Surf.*, 113(F4), 2008.
- 699 Joughin, I., Smith, B. E., and Howat, I. M.: A complete map of Greenland ice velocity derived from
700 satellite data collected over 20 years, *J. Glaciol.*, 64(243), 1-11, 2018.
- 701 Joughin, I., Smith, B. E., Howat, I. M., Scambos, T., and Moon, T.: Greenland flow variability from
702 ice-sheet-wide velocity mapping, *J. Glaciol.*, 56(197), 415-430, 2010.
- 703 Joughin, I., Smith, B., Shean, D., and Floricioiu, D.: Brief communication: Further summer speedup
704 of Jakobshavn Isbrae, *The Cryosphere*, 8, 209-214, 2014.
- 705 Krabill, W., Abdalati, W., Frederick, E., Manizade, S., Martin, C., Sonntag, J., Swift, R., Thomas,
706 R., Wright, W., and Yungel, J.: Greenland ice sheet: High-elevation balance and peripheral thinning.
707 *Science*, 289(5478), 428-430, 2000.
- 708 Lampkin, D. J., Amador, N., Parizek, B. R., Farness, K., and Jezek, K.: Drainage from water-filled
709 crevasses along the margins of Jakobshavn Isbrae: A potential catalyst for catchment expansion, *J.
710 Geophys. Res.-Earth Surf.*, 118(2), 795-813, 2013.
- 711 Luckman, A., and Murray, T.: Seasonal variation in velocity before retreat of Jakobshavn Isbrae,
712 Greenland, *Geophys. Res. Lett.*, 32(8), 2005.
- 713 Morlighem, M., Williams, C. N., Rignot, E., An, L., Arndt, J. E., Bamber, J. L., Catania, G., Chauché,
714 N., Dowdeswell, J. A., Dorschel, B., Fenty, I., Hogan, K., Howat, I., Hubbard, A., Jakobsson, M.,
715 Jordan, T. M., Kjeldsen, K. K., Millan, R., Mayer, L., Mouginot, J., Noël, B. P. Y., O’Cofaigh, C.,
716 Palmer, S., Rysgaard, S., Seroussi, H., Siegert, M. J., Slabon, P., Straneo, F., Van den Broeke, M. R.,
717 Weinrebe, W., Wood, M., and Zinglensen, K. B.: BedMachine v3: Complete bed topography and
718 ocean bathymetry mapping of Greenland from multibeam echo sounding combined with mass
719 conservation, *Geophys. Res. Lett.*, 44(21), 11-051, 2017.
- 720 Moss, R. H., Edmonds, J. A., Hibbard, K. A., Manning, M. R., Rose, S. K., Van Vuuren, D. P., Carter,
721 T. R., Emori, S., Kainuma, M., Kram, T., Meehl, G. A., Mitchell, J. F.B., Nakicenovic, N., Riahi,
722 K., Smith, S. J., Stouffer, R. J., Thomson, A. M., Weyant, J. P., and Wilbanks, T. J.: The next

- 723 generation of scenarios for climate change research and assessment. *Nature*, 463(7282), 747-756,
724 2010.
- 725 Motyka, R. J., Truffer, M., Fahnestock, M., Mortensen, J., Rysgaard, S., and Howat, I.: Submarine
726 melting of the 1985 Jakobshavn Isbræ floating mélange and the triggering of the current retreat, *J.*
727 *Geophys. Res.-Earth Surf.*, 116(F1), 2011.
- 728 Muresan, I. S., Khan, S. A., Aschwanden, A., Khroulev, C., Van Dam, T., Bamber, J., Van Den
729 Broeke, M. R., Wouters, B., Munneke, P. K., and Kjær, K. H.: Modelled glacier dynamics over the
730 last quarter of a century at Jakobshavn Isbræ, *The Cryosphere*, 10(2), 597-611, 2016.
- 731 Nick, F. M., Vieli, A., Andersen, M. L., Joughin, I., Payne, A., Edwards, T. L., Pattyn, F. and van de
732 Wal, R. S.: Future sea-level rise from Greenland's main outlet glaciers in a warming climate, *Nature*,
733 497(7448), 235, 2013.
- 734 Phillips, T., Rajaram, H., and Steffen, K.: Cryo-hydrologic warming: A potential mechanism for
735 rapid thermal response of ice sheets, *Geophys. Res. Lett.*, 37(20), 2010.
- 736 Pollard, D., and DeConto, R. M.: Description of a hybrid ice sheet-shelf model, and application to
737 Antarctica, *Geosci. Model Dev.*, 5(5), 1273, 2012.
- 738 Pollard, D., Deconto, R. M., and Alley, R. B.: Potential Antarctic ice sheet retreat driven by
739 hydrofracturing and ice cliff failure, *Earth Planet. Sci. Lett.*, 412, 112-121, 2015
- 740 Schoof, C., and Hindmarsh, R. C.: Thin-film flows with wall slip: an asymptotic analysis of higher
741 order glacier flow models, *Q. J. Mech. Appl. Math.*, 63(1), 73-114, 2010.
- 742 Shapero, D. R., Joughin, I. R., Poinar, K., Morlighem, M., and Gillet-Chaulet, F.: Basal resistance
743 for three of the largest Greenland outlet glaciers, *J. Geophys. Res.-Earth Surf.*, 121(1), 168-180,
744 2016.
- 745 Sohn, H. G., Jezek, K. C., and van der Veen, C. J.: Jakobshavn Glacier, West Greenland: 30 years
746 of spaceborne observations, *Geophys. Res. Lett.*, 25(14), 2699-2702, 1998.
- 747 Steiger, N., Nisancioglu, K. H., Åkesson, H., Fleurian, B. D., and Nick, F. M.: Simulated retreat of
748 Jakobshavn Isbræ since the Little Ice Age controlled by geometry, *The Cryosphere*, 12(7), 2249-
749 2266, 2018.
- 750 Sun, S., Cornford, S. L., Moore, J. C., Gladstone, R., and Zhao, L.: Ice shelf fracture
751 parameterization in an ice sheet model, *The Cryosphere*, 11(6), 2543-2554, 2017.
- 752 Tsai, V. C., Stewart, A. L., and Thompson, A. F.: Marine ice-sheet profiles and stability under
753 Coulomb basal conditions, *J. Glaciol.*, 61(226), 205-215, 2015.
- 754 Van Angelen, J. H., M Lenaerts, J. T., Van den Broeke, M. R., Fettweis, X., and Meijgaard, E.: Rapid
755 loss of firn pore space accelerates 21st century Greenland mass loss, *Geophys. Res. Lett.*, 40(10),
756 2109-2113, 2013.
- 757 Van Der Veen, C. J., Plummer, J. C., and Stearns, L. A.: Controls on the recent speed-up of
758 Jakobshavn Isbræ, West Greenland, *J. Glaciol.*, 57(204), 770-782, 2011.
- 759 Vieli, A., and Nick, F. M.: Understanding and modelling rapid dynamic changes of tidewater outlet
760 glaciers: issues and implications, *Surv. Geophys.*, 32(4-5), 437-458, 2011.

- 761 Watanabe, S., Hajima, T., Sudo, K., Nagashima, T., Takemura, T., Okajima, H., Nozawa, T., Kawase,
762 H., Abe, M., Yokohata, T., Ise, T., Sato, H., Kato, E., Takata, K., Emori, S., and Kawamiya, M.:
763 MIROC-ESM 2010: Model description and basic results of CMIP5-20c3m experiments, *Geosci.*
764 *Model Dev.*, 4(4), 845, 2011.
- 765 Weertman, J.: On the Sliding of Glaciers, *J. Glaciol.*, 3(21), 33-38, 1957.
- 766 Xie, S., Dixon, T. H., Voytenko, D., Holland, D. M., Holland, D., and Zheng, T.: Precursor motion
767 to iceberg calving at Jakobshavn Isbræ, Greenland, observed with terrestrial radar interferometry, *J.*
768 *Glaciol.*, 62(236), 1134-1142, 2016.